This document is the accepted manuscript version of the following article:
Marberger, A., Petrov, A. W., Steiger, P., Elsener, M., Kröcher, O., Nachtegaal, M., & Ferri, D. (2018). Time-resolved copper speciation during selective catalytic reduction of NO on Cu-SSZ-13. Nature Catalysis, 1(3), 221-227. https://doi.org/10.1038/s41929-018-0032-6

Time-resolved copper speciation during selective catalytic reduction of NO on Cu-SSZ-13

Adrian Marberger,[a,b,†] Andrey W. Petrov,[a,c,†] Patrick Steiger,[a,b] Martin Elsener,[a] Oliver Kröcher, [a,b] Maarten Nachtegaal[a,*] and Davide Ferri[a,*]

[a] Paul Scherrer Institut, CH-5232 Villigen PSI, Switzerland

[b] Ecole polytechnique fédérale de Lausanne (EPFL), Institute of Chemical Science and Engineering, CH-1015 Lausanne, Switzerland

[c] ETH Zurich, Institute for Chemical and Bioengineering, CH-8093 Zurich, Switzerland

[†] authors contributed equally

*corresponding authors:

maarten.nachtegaal@psi.ch

davide.ferri@psi.ch

ABSTRACT

Practical catalysts often operate under dynamic conditions of temperature variations and sudden changes of feed composition that call for understanding of operation and catalyst structure under analogous experimental conditions. For instance, the copper exchanged small pore SSZ-13 catalyst used currently in the selective catalytic reduction of harmful nitrogen oxides from the exhaust gas of diesel fuelled vehicles operates under recurrent ammonia dosage. Here we report the design of unsteady state experiments that mimic such dynamic environment to obtain key mechanistic information on this reaction. Through the combination of time-resolved X-ray absorption spectroscopy and transient experimentation we were able to capture an ammonia inhibition effect on the rate-limiting Cu re-oxidation at low temperature. The practical relevance of this observation was demonstrated by the optimization of the ammonia dosage on a catalyst washcoat on cordierite honeycomb, resulting in lower ammonia consumption and the increase of NO conversion at low temperature.

Introduction

Heterogeneous catalysts in practice often operate under conditions that are highly dynamic, for example continuous variation of temperature, gas composition, and gas flow rate as encountered in vehicle emission control[1,2]. Understanding the behaviour of a catalyst under these transient conditions is crucial to optimize current catalytic systems and to design future ones. However, most techniques that allow gathering of molecular level information on the structure of the catalytic active site under realistic working conditions, most notably X-ray absorption and emission spectroscopy (XAS and XES), are typically applied to study catalysts under steady state conditions. Nowadays both techniques can also be applied in time-resolved[3-5] fashion enabling the study of catalysts under dynamic non-steady state conditions. Automotive exhaust emission control systems are preferred examples for the application of these time-resolved characterization techniques due to the dynamic and complex reaction environment during driving[6-8], which includes changes into the air-to-fuel ratio, temperature, gas composition and catalyst load. In the most efficient exhaust after-treatment technology for diesel engines, the selective catalytic reduction (SCR) of nitrogen oxides by ammonia, the exhaust gas stream is enriched with ammonia (NH_3) to reduce nitrogen oxide (NO) emissions according to eq. 1[1]:

$$4NO + 4NH_3 + O_2 \rightarrow 4N_2 + 6H_2O \quad (1)$$

In recent years the copper-exchanged small pore size zeolite Cu-SSZ-13 has emerged as a commercial solution for SCR with high NO conversion at low temperature and high stability upon exposure to steam at high temperatures[9-14]. The abundant and detailed information on the structure of the active site and the reaction mechanism has been derived either by theory[15,16] or from spectroscopic experiments under steady state conditions[15-20]. Despite a few mechanistic studies including reactant cut-off and addition experiments[6,21-23], the benefits offered by time-

resolved spectroscopy have not yet been exploited to address key issues of this catalytic system, such as the rate limiting step, the nature of the active species and how transient conditions affect them.

In order to probe the dynamics of the Cu speciation and the catalyst structure-activity relation over a wide range of realistic operation conditions, we used operando X-ray absorption spectroscopy (XAS) with sub-second time resolution (0.5 s/spectrum). To mimic the necessary dynamic conditions, reactant cut-off and addition experiments were designed to cause a perturbation of the steady state[24], while the associated variations of catalytic activity were simultaneously monitored with online mass spectrometry. The time-resolved operando XAS measurements enabled us to resolve ambiguities related to the low temperature activity of low metal loaded Cu-SSZ-13. In particular, we associated the rate limiting step with the re-oxidation of Cu(I) in the low temperature regime (< 250°C), and we observed an NH_3 inhibiting effect on the re-oxidation of Cu(I). Moreover, during relaxation of the inhibition a fourfold coordinated Cu(II) species was identified as the reaction intermediate, while Cu-nitrate species appeared only when NH_3 was not further available, thus away from SCR conditions. Hence, we provide unprecedented experimental insights into the role and the stability of the different Cu species in Cu-SSZ-13 under SCR-relevant process conditions at the sub-second time scale. Finally, we demonstrate that this knowledge can directly be applied to improve the operation of actual SCR converters and to foster their future design.

Results

Low loaded Cu-SSZ-13

A Cu-SSZ-13 catalyst with low metal loading (Supplementary Method, 1.1 wt% Cu, Si/Al = 14, Cu/Al = 0.17, Supplementary Table 1) was used because its overall lower activity is beneficial to reveal peculiar features of the kinetic behaviour compared to high-loaded catalysts (Supplementary Figure 1)[16,25]. According to extended X-ray absorption fine structure spectroscopy (EXAFS, Supplementary Method) measurements in oxygen and under SCR conditions, the Cu-SSZ-13 catalyst presented primarily isolated Cu-ions (Supplementary Figure 2, Supplementary Table 2) that are indispensable for SCR on Cu-exchanged zeolites[15,19,25,26]. The selected reaction temperatures, *i.e.* 190°C, 225°C and 270°C, ensured that the measurements were performed below the characteristic temperature region between 300°C and 350°C, where low loaded Cu-SSZ-13 exhibits a significant dip in activity. This lower activity is proposed to origin from the loss of ligands around the copper ions and is likely accompanied by Cu migration within the zeolite framework[9,16,18,25].

NH_3 inhibits the rate-limiting oxidation of Cu(I) to Cu(II)

In the NH_3 cut-off experiment (**Figure** 1) representative of NH_3 dosing in a real catalytic converter, the Cu-SSZ-13 catalyst was equilibrated in SCR conditions for 30 min, followed by a rapid NH_3 cut-off initiated by automated switch valves while continuously collecting XAS spectra. The spectra were dominated by an intense white line, which is the result of a superposition of signals of various Cu-species, and by a pre-edge feature characteristic of Cu(I) species (1s→4p transition, 8982.7 eV). Normalised XAS spectra of various expected reference components[20] were used for the linear combination fit (LCF) of the time-resolved spectra

generated during the NH_3 cut-off experiment (**Figure** 2a-d, Supplementary Figures 3a, 4 and 5, Supplementary Video 1), including ionic Cu(II) attached to the zeolite framework (Cu^{II}-Z), obtained after activation of Cu-SSZ-13 at 400ºC in O_2[23]; aqueous copper nitrate species labelled as Cu^{II}-$(NO_x)_y$ because of the negligible difference between the XANES spectra of Cu^{II}-$(NO_3)_2$ and Cu^{II}-$(NO_2)_x(H_2O)_{6-x}$[21] (Supplementary Discussion); and finally, aqueous copper ammonia complexes $Cu^{I}(NH_3)_2$ and $Cu^{II}(NH_3)_4$, because NH_3 readily coordinates to Cu in Cu-SSZ-13 and forms complexes in which the Cu cation is scarcely coordinated to the zeolite framework[15,16]. The Cu speciation determined by LCF of the spectra collected under equilibrated SCR conditions (time < 0) indicated that the contribution of twofold coordinated $Cu^{I}(NH_3)_2$ decreased with increasing reaction temperature while that of Cu^{II}-Z increased with temperature (**Figure** 2a-c for 190°C, 225°C and 270°C, respectively). Only the fraction of reduced Cu(I) was dependent on the reaction temperature, which is evident by the decreasing intensity of the pre-edge feature in the XAS spectra at higher temperature under SCR conditions and its virtual disappearance at 400°C (Supplementary Figure 3c)[17]. NO conversions of ca. 17% (190°C), 42% (225°C) and 65% (270°C) were measured at the reactor cell outlet (**Figure** 2e-g).

At time zero, NH_3 was removed from the feed in order to follow the transient modifications of the local environment of Cu by XAS (**Figure** 2) and to mimic a genuine SCR system where NH_3 is dosed intermittently to the exhaust gas. The Cu speciation changed immediately after NH_3 cut-off, showing the need for the time-resolved spectroscopic approach. It is evident that the fraction of $Cu^{I}(NH_3)_2$ decreased while the Cu^{II}-Z fraction increased rapidly before adjusting to new levels. With time, all NH_3 that had been stored on the catalyst desorbed and/or reacted with NO. The oxidising nature of the feed in absence of NH_3 eventually transformed all Cu centres to Cu(II) (Cu^{II}-Z and/or Cu^{II}-$(NO_x)_y$) at all temperatures. At 190°C (**Figure** 2a), the Cu(I) species

disappeared only after the total experiment duration, whereas full oxidation was observed after ca. 1100 s at 225°C (**Figure** 2b) and after 500 s at 270°C (**Figure** 2c). In correspondence of the attainment of full Cu oxidation, the NO concentration reached 1000 ppm at increasingly shorter times with increasing reaction temperature, reflecting the faster extinction of the SCR reaction at higher temperatures (**Figure** 2e-h). At 400°C (**Figure** 2d), no reduced Cu(I) species were found in the equilibration phase under SCR conditions while Cu^{II}-Z was the dominant species that was slowly replaced by ca. 10% of Cu^{II}-$(NO_x)_y$ after NH_3 cut-off.

The high time resolution exploited in these experiments captured the dynamic behaviour of $Cu^{I}(NH_3)_2$ and $Cu^{II}(NH_3)_4$ species after NH_3 cut-off (or NH_3 addition, Supplementary Figure 6 and Supplementary Discussion). The oxidation state of the Cu species was perturbed away from the equilibrium value obtained under SCR conditions and a transient oxidation event occurred at 190°C and 225°C within 300 s and 150 s, respectively. The manifestation of this oxidation event was the increase of $Cu^{II}(NH_3)_4$ simultaneous to the decrease of $Cu^{I}(NH_3)_2$. At 270°C, the observed trend was opposite and a transient increase of $Cu^{I}(NH_3)_2$ was observed while no $Cu^{II}(NH_3)_4$ was found. Also the NO conversion (change in NO concentration, **Figure** 2e-g) immediately changed upon the NH_3 cut-off and a transient increase of conversion at low temperatures and a decrease at 270°C was observed. The changes in the XAS and the MS data occurred concurrently, which was best observed at 225°C (**Figure** 2b and **Figure** 2f).

The short-lived increase of NO conversion after the NH_3 cut-off occurring only at low temperature can be explained by the inhibiting effect of NH_3 previously observed on vanadia-titania and iron-zeolite SCR catalysts[22,27,28]. Switching off NH_3 alleviates the inhibition because NH_3 is not replenished at the Cu sites and NO can react more readily. Possible reasons for the inhibition are that NH_3 locks the Cu redox centre into Cu(I), blocks a nearby Brønsted acid

centre and/or inhibits the formation of intermediates[27]. The NO concentration and the $Cu^{I}(NH_3)_2$ speciation followed the same temporal evolution and changed at the same rate upon NH_3 cut-off (Supplementary Figures 7 and 8) indicating the close correlation of $Cu^{I}(NH_3)_2$ to the SCR process at 190°C and 225°C. At low temperature, NH_3 is thus capable of locking Cu into $Cu^{I}(NH_3)_2$, thereby hindering Cu(I) re-oxidation to Cu(II) under SCR conditions, which was proposed to occur through O_2 bonding to pairs of mobile $Cu^{I}(NH_3)_2$ species[6,16]. The transient appearance of $Cu^{II}(NH_3)_4$, best visible at 225°C, coincided with the increased SCR activity after the NH_3 cut-off (interruption of NH_3 inhibition) suggesting that $Cu^{II}(NH_3)_4$, or an analogous fourfold coordinated species (e.g. $Cu^{II}(OH)(NH_3)_3$)[6,15], is a key intermediate in the reaction mechanism at this temperature. After the sudden transient changes of the NO concentration and LCF for ca. 80 s at 225°C (**Figure** 2b and **Figure** 2f) the total fraction of Cu(II) species ($Cu^{II}(NH_3)_4$ and Cu^{II}-Z, **Figure** 2b) increased steadily because NH_3 could be supplied only from the fraction that remained adsorbed on the zeolite. As a consequence, the rate of $Cu^{II}(NH_3)_4$ formation decreased and the SCR reaction slowed down until it extinguished. The difference between the temporal evolution of Cu-species and the different rate of increase of NO conversion at NH_3 cut-off at 190°C and 225°C reflects the subtle equilibrium between NH_3 inhibition and overall activity at low temperature. Conversely, NH_3 inhibition did not occur at 270°C because NO conversion decreased at NH_3 cut-off (**Figure** 2g) and the fraction of $Cu^{I}(NH_3)_2$ increased transiently (**Figure** 2c).

In agreement with the observation by others[18,20,21,29], Cu^{II}-$(NO_x)_y$-type species were observed, however only when the catalyst was no longer fully covered by NH_3 and after the disappearance of gas phase NH_3 (**Figure** 2b and 2f). Because nitrates appeared only after the reaction environment was far away from SCR conditions, we suggest that they are either not involved in

the reaction cycle[17] or are too short-lived for XAS during SCR. The observation of Cu^{II}-$(NO_x)_y$ species is reasonable because the feed was composed of NO, O_2, H_2O and N_2 and the Cu species were fully oxidised. Our data indicate that the re-oxidation process occurred in the sequence $Cu^{I}(NH_3)_2 \rightarrow Cu^{II}(NH_3)_4 \rightarrow Cu^{II}\text{-}Z \rightarrow Cu^{II}(NO_x)_y$ suggesting that Cu nitrate species are not involved in the SCR reaction.

To follow the evolution of the various Cu species upon initiation of the SCR reaction, an experiment was conducted where NO was added to the NH_3/O_2 feed (**Figure** 3, Supplementary Figure 9). Prior to NO addition at $t < 0$, we observed that the ratio of $Cu^{II}(NH_3)_4$ and Cu^{II}-Z species was temperature dependent. The equilibrated fraction of $Cu^{II}(NH_3)_4$ changed from 40% at 190°C to 23% at 270°C while the contribution of Cu^{II}-Z passed concomitantly from 15% to ca. 40% in agreement with NH_3 desorption and the loss of coordinating NH_3 ligands with increasing temperature[19] as observed in **Figure** 2. In contrast, the amount of $Cu^{I}(NH_3)_2$ was ca. 40% irrespective of the reaction temperature, suggesting that the reduction strength of NH_3 does not change appreciably between 190-270°C and that these species are more stable than $Cu^{II}(NH_3)_4$ in this temperature regime.

The initiation of the SCR reaction upon NO addition ($t= 0$) was confirmed by the decrease of the NH_3 concentration at the reactor outlet and by the levelling of the NO concentration at ca. 80% (190°C, **Figure** 3d), 60% (225°C, **Figure** 3e) and 30% (270°C, **Figure** 3f) of the dosed value. Time-resolved changes were also detected in the LCF weights of the XAS spectra (**Figure** 3a-c) which equilibrated faster compared to the situation of **Figure** 2 because of constant NH_3 exposure. The increase of $Cu^{I}(NH_3)_2$ and the simultaneous attenuation of $Cu^{II}(NH_3)_4$ were most prominent at 190°C and 225°C (**Figure** 2a and 2b, respectively). $Cu^{II}(NH_3)_4$ was consumed by the SCR reaction, which resulted in an increased amount of stable $Cu^{I}(NH_3)_2$ species. This is in

agreement with previous reports showing the enhanced reduction of Cu sites in the presence of both NO and NH_3, compared to only NH_3[20,30]. After equilibration under SCR conditions, Cu(II) was present primarily as $Cu^{II}(NH_3)_4$ at low temperature while the coordination environment changed to Cu^{II}-Z at higher temperature (see also **Figure** 2 before NH_3 cut-off). This can be explained by the weakening of the interaction between NH_3 and Cu(II) at higher reaction temperatures[14] and the more facile reaction of $Cu^{II}(NH_3)_4$ with gaseous NO, which increased the SCR reaction rate.

The NO addition experiment depicted in **Figure** 3 enabled us to identify the rate limiting step of SCR over this low metal loaded Cu-SSZ-13 at low temperatures. The level of equilibrated $Cu^{I}(NH_3)_2$ (Cu(I):Cu(II) ratio of 75:25 at 190°C, 60:40 at 225°C and 35:65 at 270°C) decreased with increasing temperature and at 270°C it eventually remained unchanged upon NO addition compared to the preceding equilibration phase with only NH_3. The accumulation of $Cu^{I}(NH_3)_2$ at 190°C and 225°C can be explained by a slower oxidation of the Cu sites than the corresponding reduction. Assuming that the influence of diffusion limitation is negligible at these temperatures[18,31], the data presented in **Figure** 3 demonstrate that the re-oxidation of Cu(I) to Cu(II) is rate limiting. This observation agrees with the conclusion that NH_3 inhibition is at work in the same temperature range. At 270°C, the Cu(I):Cu(II) ratio was in favour of Cu^{II}-Z. If re-oxidation was still rate limiting at this temperature, the Cu(I):Cu(II) ratio would still exceed the value of 1[14]. Hence, re-oxidation is only rate limiting at 190°C and 225°C. Examination of the Cu speciation at 270°C further reveals that Cu^{II}-Z was the major Cu species. It is therefore plausible that the formation of active $Cu^{II}(NH_3)_4$ sites is limited above ca. 250°C, which can be used to explain the dip in activity above this temperature (Supplementary Figure 1).

Fate of two and four-fold coordinated Cu species

The data of **Figure** 2 and **Figure** 3 suggest that the catalyst is saturated with NH_3 during low temperature SCR and that copper forms preferably ammine complexes as long as NH_3 is provided from the gas phase or from adjacent Brønsted acid sites. The strength of these complexes decreases with increasing temperature favouring the formation of Cu^{II}-Z, as schematically shown in **Figure** 4b. At this point, it may be useful to rationalize the stability of NH_3 coordinated Cu species within Cu-SSZ-13 identified by time-resolved XAS and reflecting the catalytic activity. NH_3 desorption (**Figure** 4a) exhibits three peaks for Cu-SSZ-13 and two for H-SSZ-13[9,32,33]. The peak at ca. 170°C shifted to slightly higher temperature (ca. 190°C) when Cu-SSZ-13 was pre-oxidised (4 vol% O_2/N_2) while it greatly diminished after self-reduction in nitrogen[17,23] compared to H-SSZ-13, suggesting that the oxidation state of Cu affects the adsorption properties of NH_3 over the zeolite at low temperature. The intensity loss after self-reduction of Cu-SSZ-13 indicates a decreased fraction of oxidized copper species binding NH_3 at this temperature, revealing that this peak is related to desorption of NH_3 from $Cu^{II}(NH_3)_4$. The absence of the peak at 290°C in H-SSZ-13 and its enhancement after self-reduction of Cu-SSZ-13 strongly suggest desorption of NH_3 from $Cu^{I}(NH_3)_2$ in this region[9,32,33]. The presence of this peak in pre-oxidised Cu-SSZ-13 agrees with the partial reduction of Cu(II) to Cu(I) by NH_3[20]. The NH_3 species desorbing from the Brønsted acid sites represented by the peak at ca. 460°C[34] serves as the reservoir of adsorbed molecules, which can diffuse to the Cu sites to provide residual SCR activity upon the interruption of the NH_3 dosage. The spectroscopic experiments in **Figure** 2 and **Figure** 3 indicated that $Cu^{II}(NH_3)_4$ formed below 250°C under SCR conditions, thus lower than the desorption of NH_3 from $Cu^{I}(NH_3)_2$. On the contrary, reduced $Cu^{I}(NH_3)_2$ was observed at this temperature, which agrees well with the NH_3-TPD peak at 290°C stemming

from $Cu^{I}(NH_3)_2$. The consumption of $Cu^{II}(NH_3)_4$ during the low temperature SCR reaction leads to the formation of $Cu^{I}(NH_3)_2$, which is stable in this temperature regime as suggested by NH_3-TPD and cannot be re-oxidised quickly, making this step rate-limiting[15,16]. However, Cu(I)-NH_3 bonding weakens above 250°C, allowing occasional formation of framework coordinated Cu^{II}-Z (and possibly Cu^{I}-Z), becoming the dominant species above 350°C and likely part of a different reaction pathway not involving coordinated NH_3 species of the same nature of those observed at low temperature[15,16]. Hence, **Figure** 4 demonstrates that the SCR activity at 200-350°C follows tightly the desorption profile of NH_3 from reduced Cu sites indicating that the activity in this temperature regime is dictated by the loss of solvated Cu-ammonia species[19] and by the rate limiting re-oxidation fading off at increasing temperature. Based on these considerations, the activity of Cu-SSZ-13 can be described schematically as in **Figure** 4b. Below 250°C, copper is fully covered by NH_3 and the remarkable low temperature activity of Cu-SSZ-13 originates from the presence of $Cu^{II}(NH_3)_4$ that was best visible during the enhanced activity after the NH_3 cut-off (**Figure** 2f). Stable $Cu^{I}(NH_3)_2$ species accumulate during SCR and their re-oxidation is rate limiting, an event that possibly occurs without the loss of its NH_3 ligands[6,15,16,35]. The observed NH_3 inhibition modifies the Cu(I)/Cu(II) equilibrium by regulating the re-oxidation of $Cu^{I}(NH_3)_2$. Between 250 and 350°C, at partial NH_3 coverages, the $Cu^{II}(NH_3)_4$ species required for the low temperature SCR can no longer be formed at a sufficient rate resulting in a significant decline of the activity (**Figure** 4a). $Cu^{I}(NH_3)_2$ is still partly present because of its greater stability and can oxidise more readily to Cu^{II}-Z while NH_3 inhibition is no longer an issue in this temperature regime. Above 350ºC, the SCR reaction occurs only over framework coordinated Cu^{II}-Z, for which a different reaction mechanism may be envisaged[16] that requires a separate investigation. The transition from the low to the high temperature reaction regime is likely

accompanied by the change in the Cu configuration within the SSZ-13 framework that is widely discussed in the literature[9,15,36].

Relevance for real-world SCR converters

The molecular level findings obtained by XAS bear practical aspects. To mimic a catalytic converter analogous to those build in real SCR systems, the catalyst powder was washcoated on a cordierite monolith and was then tested in a catalytic reactor using the transient approach exploited in **Figure** 1 (**Figure** 5). Upon NH_3 cut-off from the feed at 190°C and 225°C similar to the experiments of **Figures** 1-2, the NO concentration rapidly passed through a minimum suggesting an identical NH_3 inhibition effect (**Figure** 5a). The response to the NH_3 cut-off was quicker compared to the one in **Figure** 2 due to the different flow rates and sample bed geometries. At 225°C, the SCR activity increased at a faster rate than at 190°C (**Figure** 5b), also reflecting the behaviour observed in **Figure** 2. Therefore, the NH_3 inhibition and the resulting perturbation of the Cu(I)/Cu(II) equilibrium observed by time-resolved XAS in a plug flow reactor are also valid in a realistic catalytic converter. The observation of the NH_3 inhibition on the washcoated catalyst encourages to provide recommendations to improve the low temperature activity by varying the NH_3 dosage aiming to control the influence of NH_3 inhibition and thus NH_3 slip at the catalyst outlet[37-39]. This can be realized by progressively changing the NH_3 concentration in the feed rather than dosing the same amount continuously (**Figure** 5d). This operation mode resulted in an optimized NO conversion especially in the low temperature regime (ca. 20% NO conversion with standard dosage and 36% with optimised dosage at 200°C; **Figure** 5c-d). Low NH_3 dosage is desired in real applications, e.g. catalytic converters of diesel

vehicles, to operate the system cost efficient and to meet the maximum allowed NH_3 concentration in the exhaust.

Conclusions

The time-resolved experimentation approach used in this work allowed to monitor the evolution of various Cu species in Cu-SSZ-13 and to experimentally identify crucial characteristics of the SCR catalyst in the low temperature regime: the rate limiting re-oxidation of $Cu^{I}(NH_3)_2$ is strongly influenced by NH_3 inhibition, the active $Cu^{II}(NH_3)_4$ species are mainly formed below 250°C and the modification of the active sites with increasing temperatures is driven by the loss of NH_3 coordinating Cu species. The findings were used for understanding and improving the performance of a monolithic converter analogous to those used in real-world applications. Finally, the revealed intrinsic properties of various Cu species in Cu-SSZ-13 may be useful for the rational design of more active catalysts by tuning the properties of the active Cu species with various promoters and zeolite modifications.

Methods

Synthesis of Cu-SSZ-13

The SSZ-13 zeolite with Si/Al = 14.4 was prepared by hydrothermal synthesis. First, 1.0 g of sodium hydroxide (Sigma-Aldrich, 98%) was dissolved in 80 ml of deionized water and mixed with 20 ml of trimethyladamantyl (TMAda) ammonium hydroxide solution (25 wt % in H_2O, Sachem). Then 1.56 g of aluminum hydroxide (Sigma-Aldrich, reagent grade) and 15 g of fumed silica (Sigma-Aldrich, 0.007 μm) were slowly added to the solution under vigorous stirring. The resulting gel with the molar composition $10TMAda{:}10NaOH{:}4Al_2O_3{:}100SiO_2{:}2200H_2O$ was

aged at RT for 2 h and then transferred into a stirred autoclave with teflon liner. The zeolite was hydrothermally synthesized at 160°C for 120 h, subsequently washed with acetone and deionized water, dried at 120°C for 12 h and then calcined in air at 575°C for 8 h. The crystal structure of the sample was confirmed by X-ray diffraction (Supplementary Figure 10).

The obtained solid was ion-exchanged three times with an excess of 1 M ammonium nitrate solution (Sigma-Aldrich, 98%) and calcined at 500°C for 2 h to ensure that the zeolite is in the H-form (H-SSZ-13). Finally, H-SSZ-13 was ion-exchanged with 0.1 M copper sulfate solution (Sigma-Aldrich, 98%) at 80°C for 4 h, dried at 120°C for 12 h and calcined in air at 600°C for 4 h to yield Cu-SSZ-13.

Operando X-ray absorption spectroscopy

A custom-made cell was used[40,41] for the operando XAS measurements, using ca. 17 mg of Cu-SSZ-13 (100–150 μm sieve fraction) which were firmly fixed between two quartz wool plugs (bed length, 3 mm). Graphite windows (thickness, 0.5 mm) were used on either side of the catalytic bed to ensure X-ray transmission and an air-tight reaction environment. The temperature of the cell was controlled by a thermocouple inserted ca. 0.5 mm in the catalytic bed from the inlet section of the cell to guarantee homogeneous temperatures over the entire catalytic bed. Mass flow controllers were used to generate a constant flow of the gas mixture (50 ml/min; GHSV = 100'000 h^{-1}) and automated switch valves (Parker, type Series 9; opening response time, $\leqslant$ 5 ms) installed in front of the cell enabled the execution of transient experiments. Stainless steel tubing (1/16 inch) was used throughout; the distance between the switch valves and the middle of the catalyst bed was approximately 100 mm.

Operando XAS measurements were carried out at the SuperXAS beamline of the Swiss Light Source (SLS, Villigen, Switzerland). The storage ring operated at 2.4 GeV in top-up mode with a ring current of 400 mA. The polychromatic beam was collimated by a Si-coated mirror at 2.5 mrad (which also served to reduce higher order harmonics) and subsequently monochromatized by a Si(111) channel-cut monochromator, which allowed data collection in quick scanning EXAFS (QEXAFS) mode at 2 Hz[42]. Spectra were collected in transmission mode using N_2-filled ionization chambers. A Cu reference foil mounted between the second and third ionization chamber was measured simultaneously for absolute energy calibration. The QEXAFS spectra were averaged, background corrected and normalized using the JAQ 2 software (*2*); linear combination fitting analysis (LCF) was performed using the prestopronto software[43] and in the energy range of 8965-9035 eV.

Catalytic performance test on a monolith

A washcoated Cu-SSZ-13 monolith (7x14x50 mm, 300 cells per square inch) was tested on a dedicated laboratory test reactor[37] using a feed of 10 vol% O_2, 5 vol% H_2O, 500 ppm NO and 500 ppm NH_3 (or the NH_3 dosage given in Figure 5d) with balance N_2 in order to mimic realistic exhaust gas composition. The gas hourly space velocity GHSV was 50,000 h^{-1}, which is typical for SCR converters of diesel vehicles[44]. A calibrated FT-IR spectrometer (Nexus Thermo Fisher), equipped with a heated gas cell was used for the online gas analysis of the exhaust gas. The NO_x conversion was calculated according to Supplementary Equation 1.

References

1 Nova, I. & Tronconi, E. *Urea-SCR Technology for deNOx After Treatment of Diesel Exhausts*. (Springer-Verlag New York, 2014).

2 Nunney, M. J. *Light and Heavy Vehicle Technology*. Vol. 4th ed (Routledge, 2007).

3 Lamberti, C. & van Bokhoven, J. A. *X-Ray Absorption and X-Ray Emission Spectroscopy*. (John Wiley & Sons, Ltd, 2016).

4 Kopelent, R. *et al.* Catalytically active and spectator Ce^{3+} in ceria-supported metal catalysts. *Angew. Chem. Int. Ed.* **54**, 8728-8731 (2015).

5 Singh, J. *et al.* Generating highly active partially oxidized platinum during oxidation of carbon monoxide over Pt/Al_2O_3: In situ, time-resolved, and high-energy-resolution X-ray absorption spectroscopy. *Angew. Chem. Int. Ed.* **47**, 9260-9264 (2008).

6 Paolucci, C. *et al.* Dynamic multinuclear sites formed by mobilized copper ions in NO_x selective catalytic reduction. *Science*, **357**, 898-903 (2017).

7 Newton, M. A., Belver-Coldeira, C., Martínez-Arias, A. & Fernández-García, M. Dynamic in situ observation of rapid size and shape change of supported Pd nanoparticles during CO/NO cycling. *Nat. Mater.* **6**, 528-532 (2007).

8 Nagai, Y. *et al.* In situ redispersion of platinum autoexhaust catalysts: An on-line approach to increasing catalyst lifetimes? *Angew. Chem. Int. Ed.* **47**, 9303-9306 (2008).

9 Beale, A. M., Gao, F., Lezcano-Gonzalez, I., Peden, C. H. F. & Szanyi, J. Recent advances in automotive catalysis for NO_x emission control by small-pore microporous materials. *Chem. Soc. Rev.* **44**, 7371-7405 (2015).

10 Iwamoto, M. *et al.* Copper(II) ion-exchanged ZSM-5 zeolites as highly active catalysts for direct and continuous decomposition of nitrogen monoxide. *J. Chem. Soc., Chem. Commun.*, 1272-1273 (1986).

11 Wang, J., Zhao, H., Haller, G. & Li, Y. Recent advances in the selective catalytic reduction of NO_x with NH_3 on Cu-chabazite catalysts. *Appl. Catal., B* **202**, 346-354 (2017).

12 Kwak, J. H., Tonkyn, R. G., Kim, D. H., Szanyi, J. & Peden, C. H. F. Excellent activity and selectivity of Cu-SSZ-13 in the selective catalytic reduction of NO_x with NH_3. *J. Catal.* **275**, 187-190 (2010).

13 Fickel, D. W., D'Addio, E., Lauterbach, J. A. & Lobo, R. F. The ammonia selective catalytic reduction activity of copper-exchanged small-pore zeolites. *Appl. Catal., B* **102**, 441-448 (2011).

14 Paolucci, C., Di Iorio, J. R., Ribeiro, F. H., Gounder, R. & Schneider, W. F. Catalysis science of NO_x selective catalytic reduction with ammonia over Cu-SSZ-13 and Cu-SAPO-34. *Adv. Catal.* **59**, 1-107 (2016).

15 Paolucci, C. *et al.* Catalysis in a Cage: Condition-Dependent Speciation and Dynamics of Exchanged Cu Cations in SSZ-13 Zeolites. *J. Am. Chem. Soc.* **138**, 6028-6048 (2016).

16 Gao, F., Mei, D., Wang, Y., Szanyi, J. & Peden, C. H. F. Selective Catalytic Reduction over Cu/SSZ-13: Linking Homo- and Heterogeneous Catalysis. *J. Am. Chem. Soc.* **139**, 4935-4942 (2017).

17 Gunter, T. *et al.* Structural snapshots of the SCR reaction mechanism on Cu-SSZ-13. *Chem. Comm.* **51**, 9227-9230 (2015).

18 Gao, F. *et al.* Structure–activity relationships in NH_3-SCR over Cu-SSZ-13 as probed by reaction kinetics and EPR studies. *J. Catal.* **300**, 20-29 (2013).

19 Lomachenko, K. A. *et al.* The Cu-CHA deNOx Catalyst in Action: Temperature-dependent NH_3-assisted selective catalytic reduction monitored by operando XAS and XES. *J. Am. Chem. Soc.***138**, 12025-12028 (2016).

20 Janssens, T. V. W. *et al.* A consistent reaction scheme for the selective catalytic reduction of nitrogen oxides with ammonia. *ACS Catal.* **5**, 2832-2845 (2015).

21 Tyrsted, C. *et al.* Nitrate-nitrite equilibrium in the reaction of NO with a Cu-CHA catalyst for NH_3-SCR. *Catal. Sci. Tech.* **6**, 8314-8324 (2016).

22 Doronkin, D. E. *et al.* Operando spatially- and time-resolved XAS study on zeolite catalysts for selective catalytic reduction of NO_x by NH_3. *J. Phys. Chem. C* **118**, 10204-10212 (2014).

23 Borfecchia, E. *et al.* Revisiting the nature of Cu sites in the activated Cu-SSZ-13 catalyst for SCR reaction. *Chem. Sci.* **6**, 548-563 (2015).

24 Marberger, A., Ferri, D., Elsener, M. & Kröcher, O. The significance of Lewis acid sites for the selective catalytic reduction of nitric oxide on vanadium-based catalysts. *Angew. Chem. Int. Ed.* **55**, 11989-11994 (2016).

25 Gao, F. *et al.* Understanding ammonia selective catalytic reduction kinetics over Cu/SSZ-13 from motion of the Cu ions. *J. Catal.* **319**, 1-14 (2014).

26 Zhang, T., Qiu, F., Chang, H., Li, X. & Li, J. Identification of active sites and reaction mechanism on low-temperature SCR activity over Cu-SSZ-13 catalysts prepared by different methods. *Catal. Sci. Tech.* **6**, 6294-6304 (2016).

27 Nova, I., Ciardelli, C., Tronconi, E., Chatterjee, D. & Bandl-Konrad, B. NH_3-SCR of NO over a V-based catalyst: Low-T redox kinetics with NH_3 inhibition. *AIChE J.* **52**, 3222-3233 (2006).

28 Auvray, X. *et al.* Local ammonia storage and ammonia inhibition in a monolithic copper-beta zeolite SCR catalyst. *Appl. Catal., B* **126**, 144-152 (2012).

29 Lezcano-Gonzalez, I. *et al.* Determination of the nature of the Cu coordination complexes formed in the presence of NO and NH_3 within SSZ-13. *J. Phys. Chem. C* **119**, 24393-24403 (2015).

30 Paolucci, C. *et al.* Isolation of the copper redox steps in the standard selective catalytic reduction on Cu-SSZ-13. *Angew. Chem. Int. Ed.* **53**, 11828-11833 (2014).

31 Metkar, P. S., Balakotaiah, V. & Harold, M. P. Experimental study of mass transfer limitations in Fe- and Cu-zeolite-based NH_3-SCR monolithic catalysts. *Chem. Engin. Sci.* **66**, 5192-5203 (2011).

32 Luo, J. *et al.* New insights into Cu/SSZ-13 SCR catalyst acidity. Part I: Nature of acidic sites probed by NH_3 titration. *J. Catal.* **348**, 291-299 (2017).

33 Su, W., Li, Z., Peng, Y. & Li, J. Correlation of the changes in the framework and active Cu sites for typical Cu/CHA zeolites (SSZ-13 and SAPO-34) during hydrothermal aging. *PCCP* **17**, 29142-29149 (2015).

34 Lonyi, F. & Valion, J. A TPD and IR study of the suface species formed from ammonia on zeolite H-ZSM-5, H-mordenite and H-beta. *Thermochim. Acta* **373**, 53-57 (2001).

35 Delahay, G., Kieger, S., Tanchoux, N., Trens, P. & Coq, B. Kinetics of the selective catalytic reduction of NO by NH_3 on a Cu-faujasite catalyst. *Appl. Catal., B* **52**, 251-257 (2004).

36 Deka, U. *et al.* Confirmation of isolated Cu^{2+} ions in SSZ-13 zeolite as active sites in NH_3-selective catalytic reduction. *J. Phys. Chem. C* **116**, 4809-4818 (2012).

37 Kleemann, M., Elsener, M., Koebel, M. & Wokaun, A. Investigation of the ammonia adsorption on monolithic SCR catalysts by transient response analysis. *Appl. Catal., B* **27**, 231-242 (2000).

38 Kröcher, O. *et al.* Investigation of the selective catalytic reduction of NO by NH_3 on Fe-ZSM5 monolith catalysts. *Appl. Catal., B* **66**, 208-216 (2006).

39 Zhao, Y., Hu, J., Hua, L., Shuai, S. & Wang, J. Ammonia storage and slip in a urea selective catalytic reduction catalyst under steady and transient conditions. *Ind. Eng. Chem. Res.* **50**, 11863-11871 (2011).

40 Chiarello, G. L., Nachtegaal, M., Marchionni, V., Quaroni, L. & Ferri, D. Adding diffuse reflectance infrared Fourier transform spectroscopy capability to extended x-ray-absorption fine structure in a new cell to study solid catalysts in combination with a modulation approach. *Review of Scientific Instruments* **85**, 074102 (2014).

41 Marchionni, V., Kambolis, A., Nachtegaal, M., Kröcher, O. & Ferri, D. High energy X-ray diffraction and IR spectroscopy of Pt/Al_2O_3 during CO oxidation in a novel catalytic reactor cell. *Catalysis, Structure & Reactivity* **3**, 71-78 (2017).

42 Müller, O., Nachtegaal, M., Just, J., Lützenkirchen-Hecht, D. & Frahm, R. Quick-EXAFS setup at the SuperXAS beamline for in situ X-ray absorption spectroscopy with 10 ms time resolution. *J. Synchrotron Radiat.* **23**, 260-266 (2016).

43 Figueroa, S. J. A. & Prestipino, C. PrestoPronto: a code devoted to handling large data sets. *J. Phys. Conf. Ser.* **712**, 012012 (2016).

44 Koebel, M., Elsener, M. & Madia, G. Recent Advances in the Development of Urea-SCR for Automotive Applications. *SAE Tech. Pap.*, 3625 (2001).

Data Availability

All data that support the plots within this manuscript and other findings of this study are available from the corresponding authors upon reasonable request.

Acknowledgments

The financial support from the Swiss National Science Foundation (SNF) and from the Competence Center for Materials Science and Technology (CCMX) is kindly acknowledged.

Author Contributions

A.M. and A.W.P. designed experiments, analysed data, performed LCF of the XAS data, prepared the catalysts; P.S. performed catalytic tests and analysed data; D.F., M.N. and O.K. led the project; D.F. and M.N. designed experiments and analysed data; all authors discussed results and contributed to writing the manuscript.

Competing Financial Interests

We declare no competing financial interests.

Corresponding author

Correspondence to: Davide Ferri or Maarten Nachtegaal

Figure captions

Figure 1. Cu K-edge XANES spectra of Cu-SSZ-13 during transient experiments. Pre-edge and white line region of the operando time-resolved Cu K-edge QEXAFS spectra of Cu-SSZ-13 at (a) 190°C, (b) 225°C and (c) 270°C. All spectra are normalised. After equilibration in SCR conditions (1000 ppm NH_3, 1000 ppm NO, 6 vol% O_2, 2 vol% H_2O and make-up N_2) for 30 min, XAS data were collected in SCR conditions for 60 s (120 spectra) followed by continuous data collection in absence of NH_3 (t = 0, 0.5 s/spectrum).

Figure 2. Switching off the SCR reaction by NH_3 removal. Dynamic copper speciation obtained from linear combination fit of time-resolved QEXAFS spectra during the cut-off of 1000 ppm NH_3 from a constant flow of 1000 ppm NO, 6 vol% O_2, 2 vol% H_2O and make-up N_2 at (a) 190°C, (b) 225°C, (c) 270°C and (d) 400°C. (e-h) Corresponding MS signals of NH_3 (m/z= 17) and NO (m/z= 40). Prior to NH_3 cut-off, the catalyst was equilibrated in SCR conditions for 30 min.

Figure 3. Initiation of the SCR reaction by NO addition. Dynamic copper speciation obtained from linear combination fit of time-resolved QEXAFS spectra during the addition of 1000 ppm NO to a constant flow of 1000 ppm NH_3, 6 vol% O_2, 2 vol% H_2O and make-up N_2 at 190°C (a), 225°C (b) and 270°C (c). (d-f) Corresponding MS signals of NH_3 (m/z = 17) and NO (m/z = 40). Prior to NO addition, the catalyst was equilibrated in NH_3 for 30 min.

Figure 4. Temperature dependent evolution of Cu-species. (a) NO conversion of Cu-SSZ-13 measured in a laboratory test reactor for monolithic catalysts and NH_3 temperature programmed desorption (NH_3-TPD) of Cu-SSZ-13 and H-SSZ-13 after pre-oxidation in 4 vol% O_2/N_2 (full lines) and after self-reduction in N_2 at 600°C (dashed lines). (b) Schematic temperature dependence of copper speciation in Cu-SSZ-13.

Figure 5. Optimization of NH_3 dosage in monolithic catalytic converters. (a) NO and NH_3 concentrations and (b) corresponding NO conversion of washcoated Cu-SSZ-13 before and after cut-off of 500 ppm NH_3 from the SCR feed at 190°C and 225°C; (c) temperature dependence of NO conversion. For the standard conversion, an equimolar 500 ppm NH_3 and 500 ppm NO gas feed was used that included 10 vol% O_2, 6 vol% H_2O and make-up N_2. For the optimized conversion, the NH_3 dosage was varied as indicated in (d). (d) NH_3 dosage required to achieve the NO conversion values of (c).

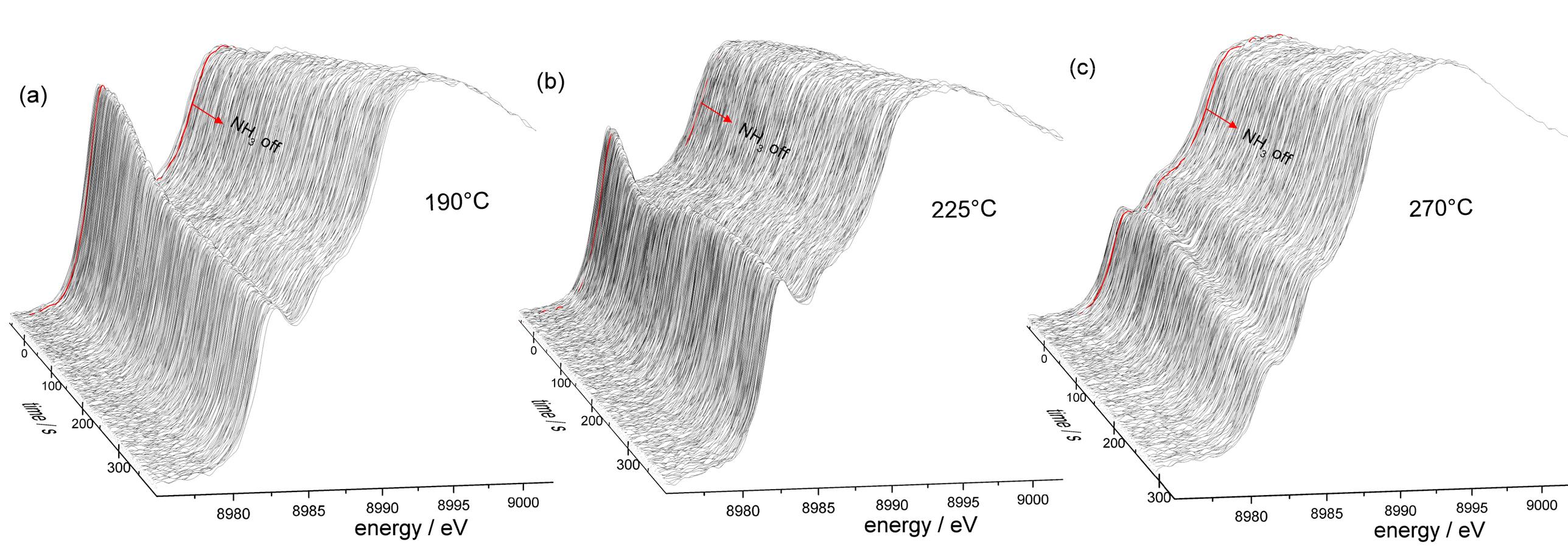
(a)
NH3 off
190°C
0
100
200
300
time / s
8980
8985
8990
8995
9000
energy / eV
(b)
NH3 off
225°C
0
100
200
300
time / s
8980
8985
8990
8995
9000
energy / eV
(c)
NH3 off
270°C
0
100
200
300
time / s
8980
8985
8990
8995
9000
energy / eV

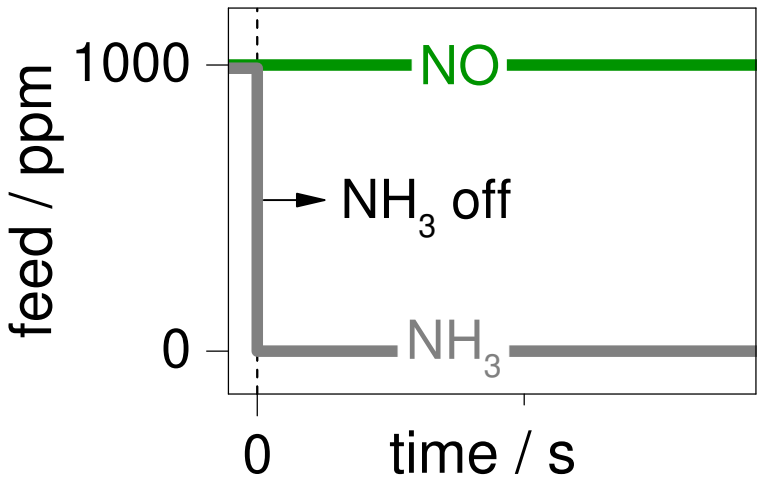
feed / ppm
1000
0
NO
NH3 off
NH3
0
time / s

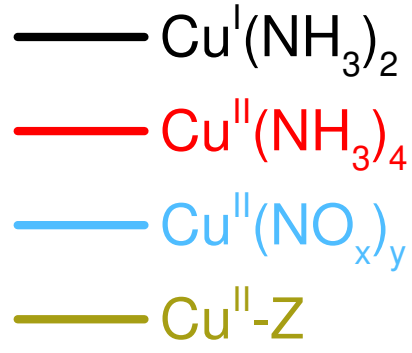
Cu^I(NH3)2
Cu^II(NH3)4
Cu^II(NOx)y
Cu^II-Z

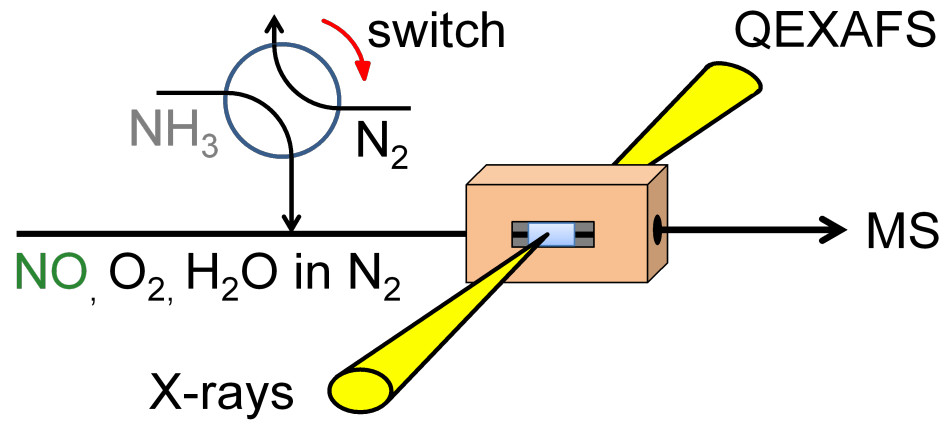
switch
QEXAFS
NH3
N2
MS
NO, O2, H2O in N2
X-rays

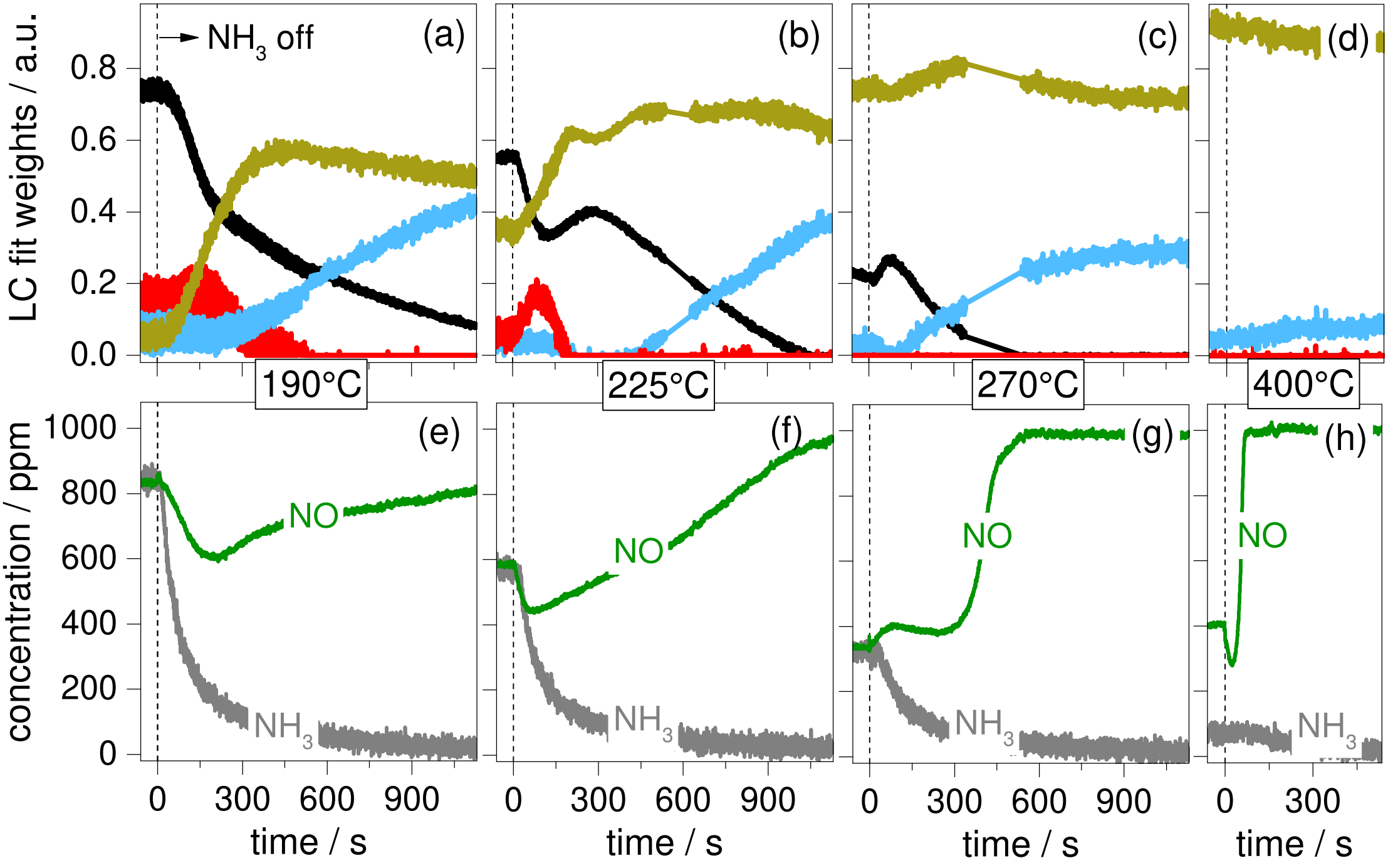
LC fit weights / a.u.
0.0
0.2
0.4
0.6
0.8
NH3 off
(a)
(b)
(c)
(d)
190°C
225°C
270°C
400°C
concentration / ppm
0
200
400
600
800
1000
NO
NH3
(e)
(f)
(g)
(h)
0
300
600
900
time / s

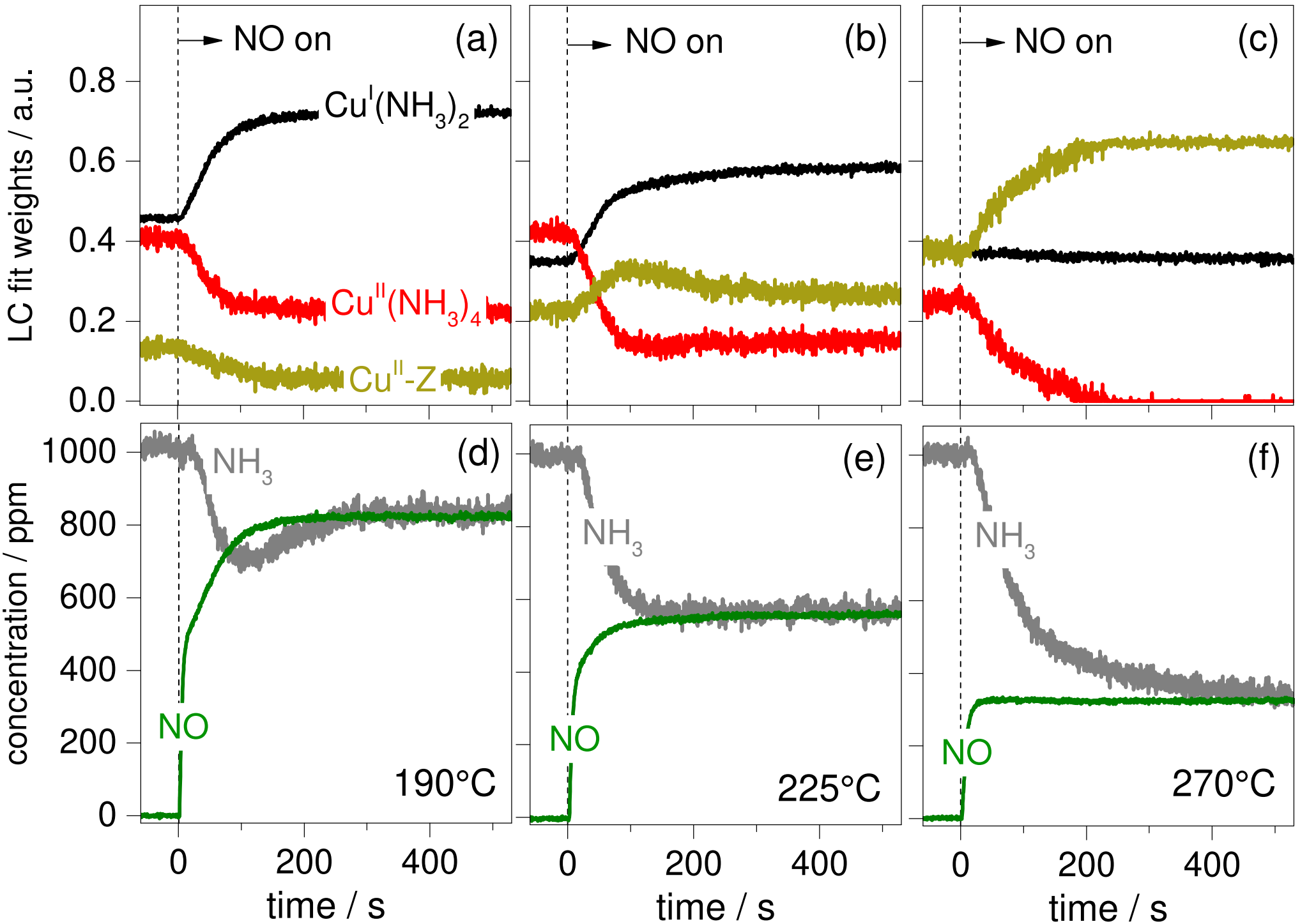
NO on
(a)
(b)
(c)
LC fit weights / a.u.
0.0
0.2
0.4
0.6
0.8
Cu^I(NH3)2
Cu^II(NH3)4
Cu^II-Z
(d)
(e)
(f)
concentration / ppm
0
200
400
600
800
1000
NH3
NO
190°C
225°C
270°C
0
200
400
time / s

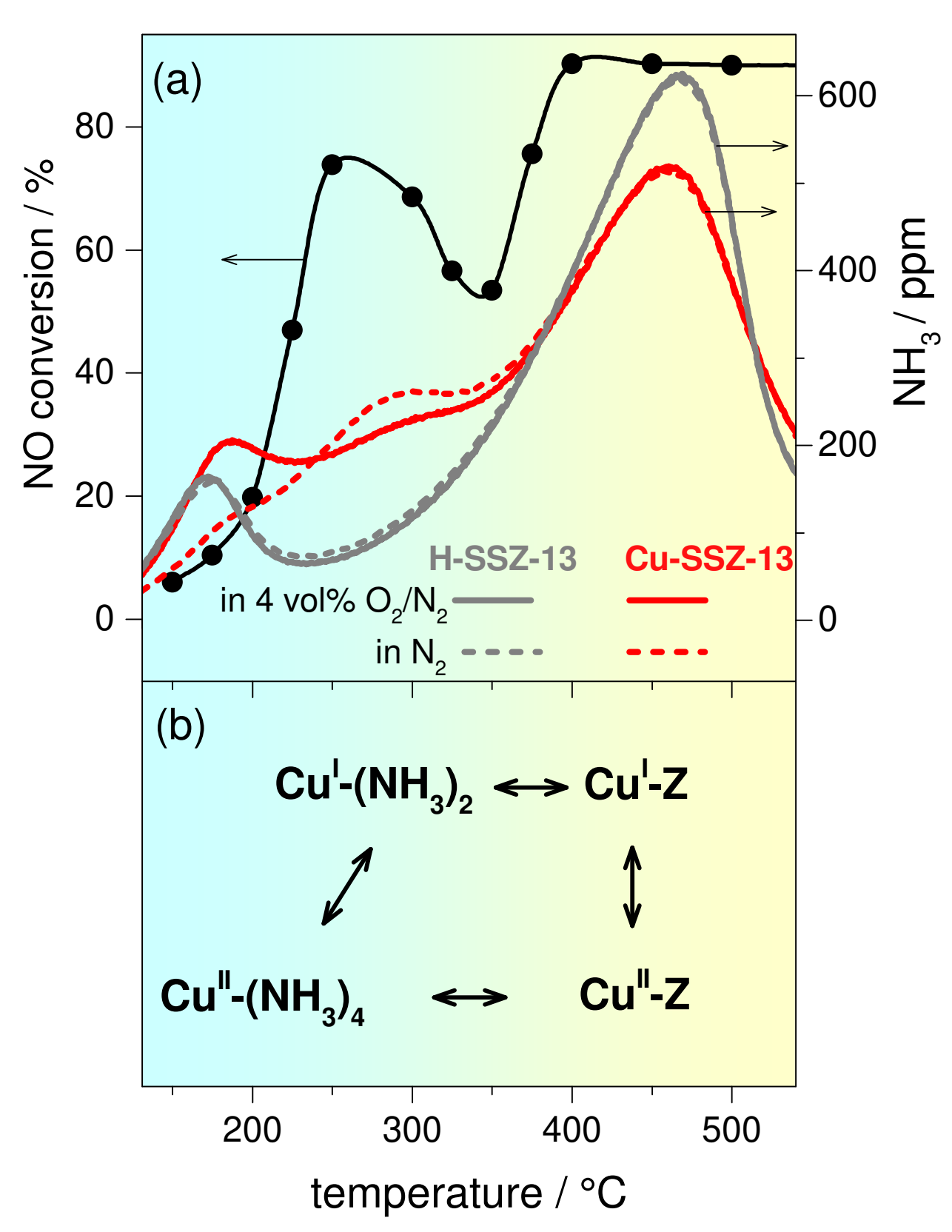
(a)
NO conversion / %
80
60
40
20
0
600
400
200
0
NH3 / ppm
H-SSZ-13
Cu-SSZ-13
in 4 vol% O2/N2
in N2
(b)
Cu^I-(NH3)2
Cu^I-Z
Cu^II-(NH3)4
Cu^II-Z
200
300
400
500
temperature / °C

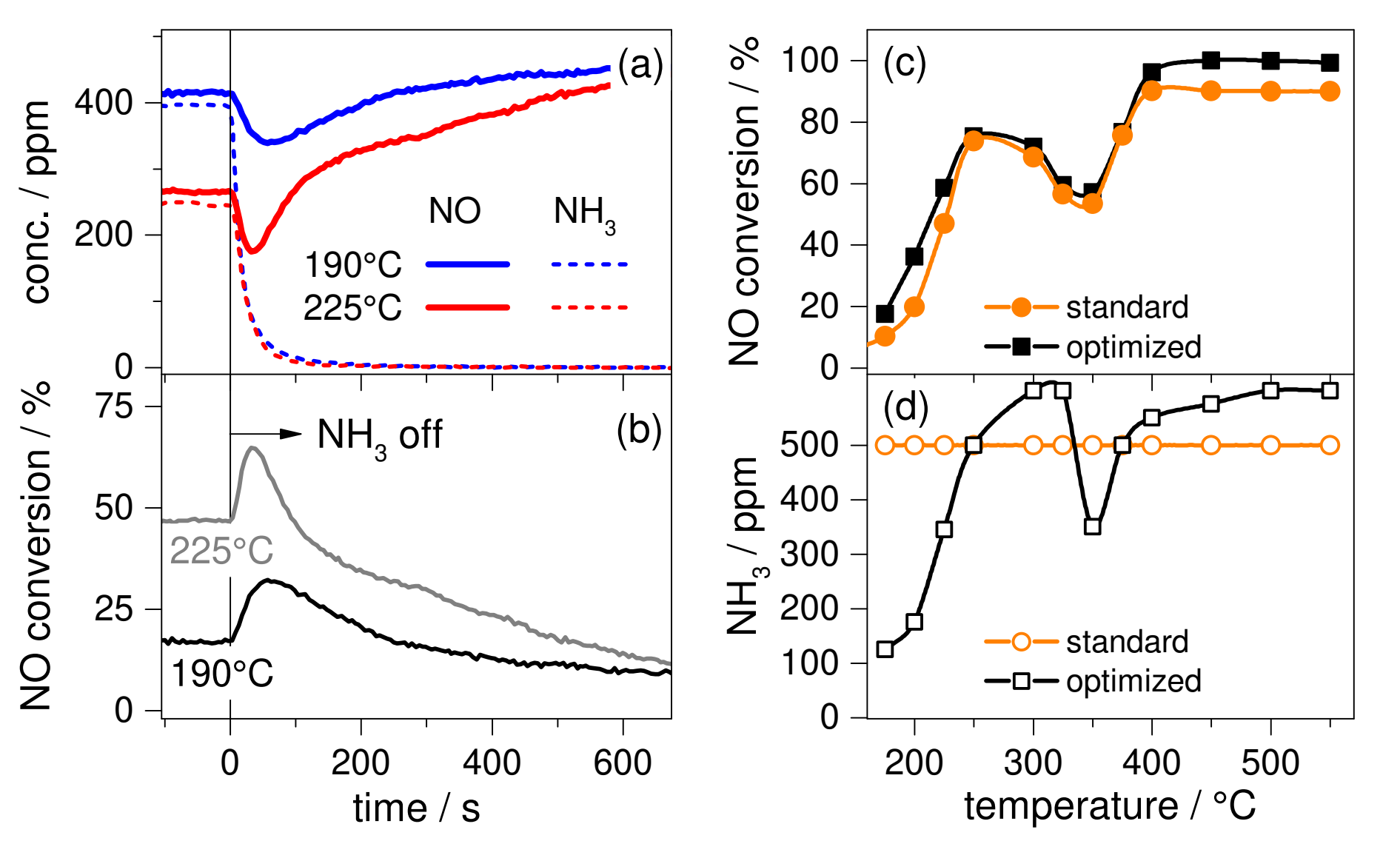
(a)
conc. / ppm
400
200
0
NO
NH3
190°C
225°C
(b)
NO conversion / %
75
50
25
0
NH3 off
225°C
190°C
0
200
400
600
time / s
(c)
NO conversion / %
100
80
60
40
20
0
standard
optimized
(d)
NH3 / ppm
500
400
300
200
100
0
standard
optimized
200
300
400
500
temperature / °C